Stress-Dependent Fluid Dynamics of Shale Gas Reservoirs: A Pore Network Modeling Approach

Jalal Foroozesh[1,2]*, Amr Ibrahim Mohamed Abdalla[3], Davood Zivar[4], Jalal Douraghinejad[5]

[1] School of Energy and Electronic Engineeirng, Portsmouth, UK

[2] Institute of Hydrocarbon Recovery, Universiti Teknologi PETRONAS, Perak, Malaysia

[3] Petroleum Engineering Department, Universiti Teknologi PETRONAS, Perak, Malaysia

[4] Department of Petroleum Engineering, School of Mining and Geosciences, Nazarbayev University, Nur-Sultan, Kazakhstan

[5] Geosciences Department, Universiti Teknologi PETRONAS, Perak, Malaysia

*Corresponding author email: jalal.foroozesh@gmail.com; jalal.foroozesh@port.ac.uk

Abstract

In this study, the pore network modeling approach is implemented to study the flow behavior of the methane gas in shale reservoirs in the presence of slip flow and gas desorption under different effective stress conditions through the effect on apparent permeability. A single pore and a pore network are constructed using a down-scaled Berea sandstone image. The compressible Stokes is applied with proper boundary conditions to capture slip flow and gas desorption effects. To include the effect of stress, poroelasticity principles are applied to describe the interaction between fluid flow and solid deformation. The model performance is verified against an experimental data taken from the literature. Both models show a negative effect of stress on gas flow when slip flow and desorption mechanisms are activated in the models. In the single pore model, slip has a positive and complementary effect on desorption at a specific stress value when their coupled contributions are summative. However, the results

of pore network model show that slip has a destructive effect on desorption contribution specially at low effective stress values. That is, the changes in pore pressure induced by the slip mechanism act to limit the desorption contribution. This is clearly noted with the consideration of stress effects. At high effective stress values, the slip effect is limited due to the increase in pore pressure by compression, hence a closer matching between the permeability enhancement produced by the desorption mechanism alone and the coupled effect of desorption and slip can be noticed. Stress acts to limit the slip flow and also the desorption mechanism as they both are a function of pore pressure, however, as stress increases the contribution of desorption no longer would be reduced by slip flow. This study provides insights into stress role in multiphysics gas flow in shale reservoirs.

Keywords: Pore network modeling; Shale reservoirs; Gas desorption; Slip flow; Effective stress; Apparent permeability

1. Introduction

Shale gas reservoirs are categorized under unconventional resources, where low porosity, ultra-low permeability, nanoscale pore and pore throat radius, stress dependency of the inherent properties, and complex gas flow mechanisms are listed as the technical issues of these reservoirs [1]. Despite the mentioned complexities, a large amount of natural gas all around the world is produced from shale gas reservoirs, especially in the United States (34% based on the EIA report in 2011) [2].

The permeability of the shale gas reservoirs is within the range of ultra-low (several nano-Darcy to several hundred nano-Darcy) and it varies with the effective stress of porous media. This range of permeability is representative of the nanoscale pore and pore throat size, which

are close to the mean free path of the molecules. Thus, several flow regimes, such as continuum flow, slip flow, transitional flow, and molecular-free flow, are expected to occur during the different stages of production [3]. The mentioned flow regimes are classified using the Knudsen number, where it describes the frequency collisions of molecule-molecule and molecule-wall based on the theory of the gas molecular dynamics [4, 5], as presented in Table 1.

Table 1. The flow regimes and their corresponding Knudsen numbers [3]

Flow regime	Knudsen number (K_n)
Continuum flow	$0 - 10^{-3}$
Slip flow	$10^{-3} - 10^{-1}$
Transition flow	$10^{-1} - 10^{+1}$
Free-molecular flow	$10^{+1} - \infty$

As mentioned above, different flow regimes occur during the different stages of the production from a shale gas reservoir that can significantly affect its apparent permeability. The expression between gas slip flow phenomena and apparent permeability was introduced by Klinkenberg for the first time [6]. After that, a new line of research on the relation between slip flow and apparent permeability has been flourished, while in recent years it was studied by many researchers. For instance, Beskok and Karniadakis (1999) described different flow regimes by a comprehensive model based on the Knudsen number and the Hagen-Poiseuille equation. The proposed model can cover continuum flow, slip flow, transitional flow, and molecular-free flow regimes in micro and nano scales [5]. Later on, Civan (2010) developed

61 an equation to describe the behavior of permeability based on the Beskok and Karniadakis'
62 equation [7]. Javadpour et al. (2007 and 2009) introduced a model for the behavior of apparent
63 permeability of nanopores when Knudsen diffusion and slip flow are presented [8, 9].

64 The major portion of the gas in-place of shale gas reservoirs is found as free gas and or
65 adsorbed gas, while a small portion of it is dissolved in the formation water. Alongside with
66 different flow regimes, adsorption mechanism affects the performance of the shale gas
67 reservoirs by altering petrophysical properties of porous media, such as effective pore radius,
68 effective porosity, apparent permeability. Due to the importance of the adsorption, several
69 researchers have studied this phenomenon, where the surface diffusion is introduced as an
70 intrinsic property of gas by Fathi and Akkutlu (2009) and (2012) [10, 11]. The range of
71 1.55×10^{-7}-8.80×10^{-6} m^2/s is reported by Kang et al. (2011) for the surface diffusivity of the
72 kerogen pore surface [12]. Furthermore, the Langmuir theorem is usually applied to capture
73 the effect of adsorption by using Langmuir-Freundlich (L-F) equation and modified Langmuir
74 (M-L) [13-15]. In another study, She et al. (2014) showed that apparent permeability would be
75 affected by adsorption significantly, especially in low-pressure conditions [16]. Wang et al.
76 (2016) showed that ignoring the changes in the petrophysical properties of porous media due
77 to adsorption/desorption cause an overestimation of original gas in-place and gas production
78 rate [17]. Zhang et al. (2018) proposed a permeability model with considering the Knudsen
79 diffusion, viscous flow, and the surface diffusion of adsorbed gas. They figured out that, at a
80 low-pressure condition, pore radius and temperature would affect the apparent permeability
81 [18]. Foroozesh et al. (2019) studied the effect of slip flow and gas adsorption on the apparent
82 permeability of a set of Eagle Ford and Barnett shale samples through a pore network model.
83 It was concluded that the effect of desorption is more significant compared to slip flow on
84 altering the permeability. Additionally, it was shown that the slip effect was able to reduce the

85 effect of desorption due to a reducuction in pressure drop upoun activating slip flow in their
86 model [19].

87 In addition to the mentioned active mechanisms during gas flow, the governed in-situ
88 stresses play an important role in the shale gas reservoirs. Porous material can be described as
89 a solid structure with an internal structure consisting of connected and isolated void spaces that
90 can hold fluids. Reservoirs consist of this solid matrix as well as the hydrocarbon held within
91 the network of pores, both existing at a state of pressure equilibrium before production. As
92 extraction of hydrocarbon commences, the change in pressure equilibrium induces a transfer
93 of stress to the solid network causing the deformation of the solid matrix that can lead to a
94 reduction in pore spaces. The reduction in pore volume alters the pressure equilibrium once
95 more pushing out the hydrocarbons within the pores creating an iterating loop of events. This
96 brings us to the law of effective stress which states that this coupled behavior is a function of
97 applied stress and pore pressure [20]. The deformations that occurred within the solid frame
98 are due to effective stress. The dynamic interaction between fluid flow and stress can be
99 described using a set of governing equations formulated based on Biot's poroelasticity theory
100 [21]. Induced deformations are described through a set of constitutive equations of linear
101 elasticity.

102 Many present studies have taken stress effects into consideration while assessing the
103 permeability of either conventional or unconventional reservoirs [22-25]. This is usually
104 through experimental tests conducted on shale core samples to correlate effective stress and
105 permeability. Various logarithmic and empirical equations [26, 27] as well as exponential
106 functions [28-31] have been used to describe the relationship. In a work done by Yang et al.
107 (2017), Klinkinberg's model was extended to a stress-dependent permeability model. The

effects of confining pressure on permeability reduction were noted by Soeder (1988) [32]. A study by Gutierrez et al. (2015) also concluded that a large reduction in fracture permeability occurs as effective normal stress is increased [33]. Bustin et al. (2008) estimated the permeability of Barnett, Muskwa, and Ohio shale core samples under confining pressures ranging up to 40 MPa. They found an exponential relationship between the shale permeability and effective stress [34]. Similarly, Dong et al. (2010) carried out several experimental tests on Chinsui shale core samples located in Taiwan under a confining pressure range up to 120 MPa. Although an exponential relationship was shown at lower confining pressures (up to 40 MPa), at higher confining pressures this behavior was no longer maintained as it was more adequately fitted with the power law. This shift in behavior could be due to the mechanical properties of shale rocks [23]. Wentong et al. (2018) conducted a study on the stress sensitivity of shale reservoirs. Their findings showed that pore compressibility shares a negatively linear relationship with the rocks Young's modulus. It was observed that, at higherYoung's modulus values, pore compressibility would decrease. [35].

In addition, a few studies have been done on the modeling aspects of the permeability stress-dependency in shale gas reservoirs. Nazari Moghaddam and Jamiolahmady (2016) studied the effect of stress and slippage on the permeability of shale gas reservoirs. At constant effective stress, a permeability enhancement was reported when pressure decreased due to gas slippage phenomena [36]. Sun et al. (2017) developed a model for apparent permeability of the nanotubes based on the Beskok and Karniadakis' equation, which shows a significant effect of stress on the transport capacity [37]. Feng et al. (2019) showed one order of magnitude reduction of the apparent permeability due to the effect of stress when slip flow, Knudsen flow, and surface diffusion are contributing to a nanoscale model [38].

When it comes to pore-scale simulation, pore network modeling provides an effective way to simulate the different physical and chemical phenomena, such as deep bed filtration, non-Darcy flow, multiphase flow, reactive flow, and non-Newtonian displacement [39, 40]. Fatt (1956) used pore network modeling for simulation of the capillary pressure curve as a function of saturation for the first time [41]. After that, pore network modeling gets high attention in different fields by researchers. For example, many researchers have tried to study fluid dynamics by considering the effect of slip flow and Knudsen diffusion for the shale gas reservoirs [8, 42-44]. The Hagen-Poiseuille equation is usually used in these studies for simplification and saving computational cost, where it can reduce the accuracy of results. Nevertheless, the Navier-Stock equation has also been used instead of the Hagen-Poiseuille equation by scholars [19].

To the best of the authors' knowledge, a detailed pore network modeling study with considering the slip flow regime, desorption of gas, and the effect of stress on the shale gas permeability, has not been presented in the literature. Therefore, the objective of this study is to use pore-scale models to investigate the contribution of slip flow and adsorption/desorption to shale gas permeability while considering stress effects. In other words, this study aims to investigate the apparent permeability of the shale rocks at different effective stress values when slip flow and gas desorption are present. This study helps to have a better and realistic understanding of gas flow behavior in shale rocks. Considering above-mentioned physics simultaneously applied on the heterogenous network of pores and flow channels in the model, it provides a more accurate tool for sound management of gas production from shale reservoirs.

To do so, a single pore and a pore network models were established using the pore structure image of a Berea sandstone sample. The unsteady-state Stocks equation was used rather than

154 the Hagen-Poiseuille equation to capture the effect of fluid compressibility. Slip flow and gas
155 adsorption were included in the models by adapting appropriate boundary conditions. To
156 include the effect of stress, the solid deformation physics was included through the
157 poroelasticity term. Coupling fluid flow and stress will help to have a solid understanding of
158 apparent permeability alteration in shale gas reservoirs.

159 2. Methodology

160 Although the shale gas reservoirs have pores and throats size in the nanoscale, various ranges
161 are reported for the size of pores and throats by researchers. For example, Cipolla et al. (2009)
162 reported 1-200 nm as a typical range for pore diameters, while the reported size of the pore
163 diameters by Sakhaee-Pour and Bryant (2012) was 5 to 20 nm [45, 46]. Pore throats are
164 considered as connecting throats with the main resistance to flow. The average size of the pore
165 throats is in the range of 1-10 nm. Therefore, considering a valid range of size for the pores
166 and pore throats plays an important role in the simulation of the fluid flow in porous media.
167 This study is initially conducted on a single pore to quantify the effects of the physical
168 phenomena and flow mechanisms without the complexities of pore geometry. The geometry
169 of the single pore consists of four grains with a minimum pore throat diameter of 5 nm and a
170 length of 24 nm (Figure 1). Then, it is extended to a pore network by using an image of a Brea
171 sandstone pore structure when it is down scaled to the nanoscale (Figure 2). The dimension of
172 the pore network model in the x-direction and the y-direction is 705 nm and 352 nm,
173 respectively. In addition, the diameters of the pores are within the range of 5-20 nm.

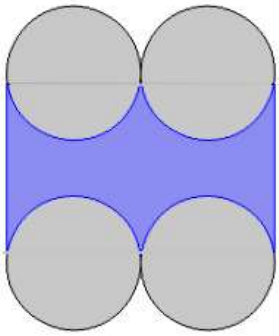

Figure 1. The geometry of the single pore model. The pathway of the fluid flow is highlighted by the blue color.

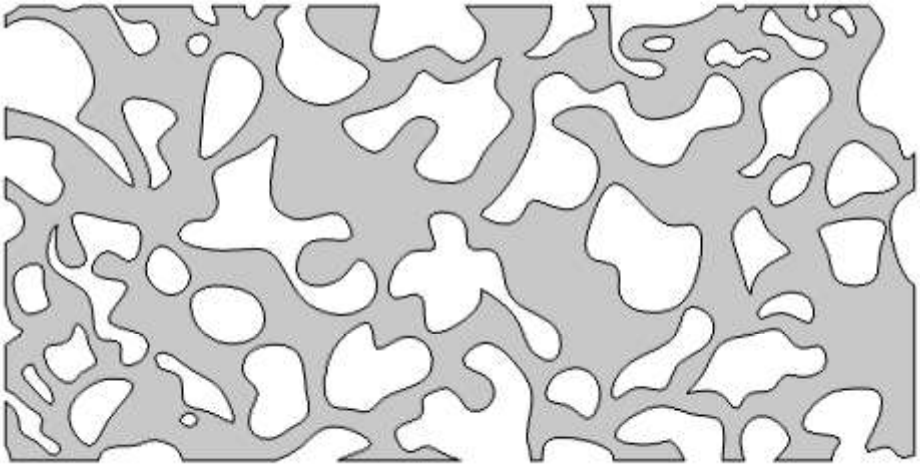

Figure 2. The constructed pore network model. The white and the grey colors represent the grains and the pores/throats, respectively [47]

When the size of the pores and pore throats of a porous media is comparable to or smaller than the mean free path of the flowing fluid, the Knudsen diffusion is getting attention. To ensure that the flow regime remains in the range of slip flow, the Knudsen number values are calculated based on the applied pore pressure and size of the pores. There are two more benefits to this issue. The first one is to exclude the Knudsen diffusion flow, and the second one is to to maintain the validity of the Stokes flow. Figure 3 shows the Knudsen number with respect to the pore diameter for different applied pore pressures. The results show the calculated Knudsen numbers are in the range of continuum to slip flow.

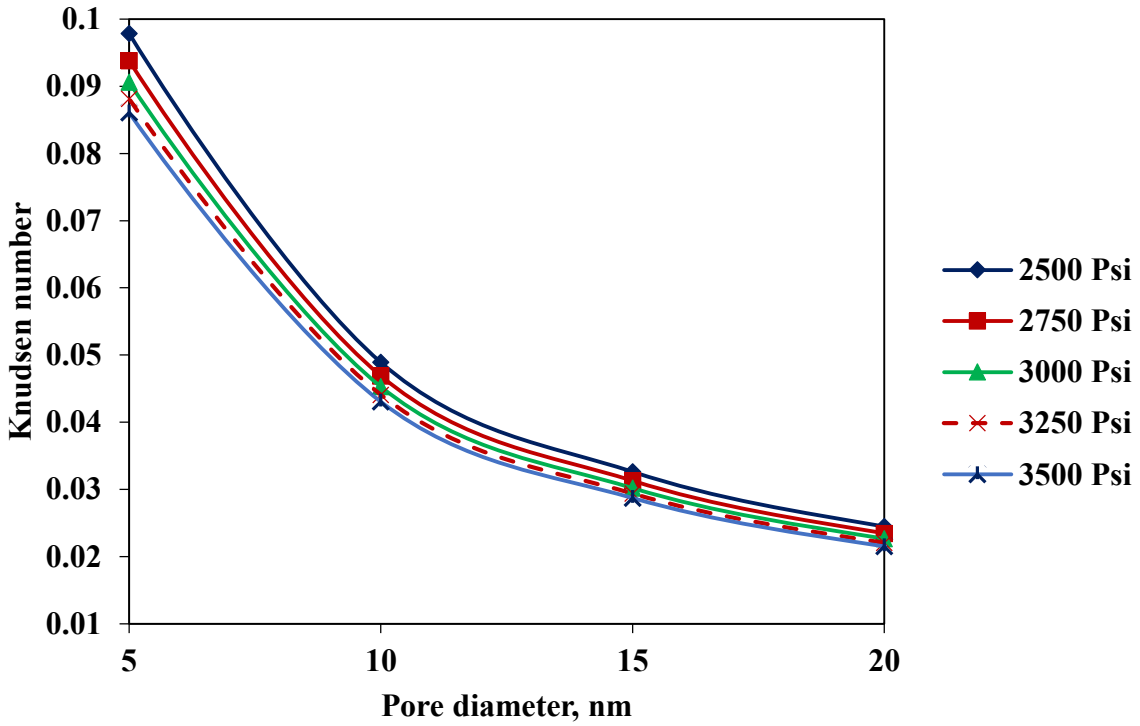

Figure 3. Knudsen number with respect to pore diameters for different pore pressures embedded in the pore network studied for methane as a real gas.

As mentioned, the flow regime is different at any given time of the life of a shale gas reservoir. It is governed by different parameters, such as reservoir pressure, geometrical aspects of the reservoir, and reservoir temperature. Based on the model setup applied in this work, the viscous flow with slip boundary conditions together with the desorption mechanism and stress effects are considered. In addition, the below assumptions are made in this study to establish a more reliable study and save the computational cost.

- The pores are fully saturated by methane (single phase).
- The methane is compressible, and its density and viscosity vary with pressure.
- The temperature is constant (40 ˚C).
- The gravity force is ignored (horizontal system).

As mentioned before, viscous flow plays a critical role to capture the fluid flow. To do so, the Navier-Stokes equation is used for the fluid flow of a viscous compressible Newtonian fluid, as presented in Eq. 1 [48].

$$\rho\left(\frac{d\vec{u}}{dt}+\vec{u}\cdot\nabla\vec{u}\right)=-\nabla p+\mu\nabla^2\vec{u}+\frac{1}{3}\mu\nabla(\nabla\cdot u) \quad (1)$$

where ρ presents the density of the fluid in kg/m^3, $\vec{u}$ stands for the velocity field, p presents the pressure in Pa, and μ presents the gas viscosity in Pa.s.

The inertial force is negligible for the presented system of pores and throats because of its nanoscale. Therefore, the Navier-Stokes equation in the form of Eq.1 can be rewritten in the form of Eq.2 (Stokes equation) when the inertial force is negligible [49].

$$\rho\left(\frac{d\vec{u}}{dt}\right)=-\nabla p+\mu\nabla^2\vec{u}+\frac{1}{3}\mu\nabla(\nabla\cdot u) \quad (2)$$

The terms density (ρ) and viscosity (μ) in Eq.2 are varied with pressure. Eq.3 and Eq.4 present the variation of density and viscosity with pressure, which are obtained based on the non-linear regression of NIST chemistry webbook data [50]. It is worth mentioning that Eq.3 and Eq.4 are valid within the range of 1 MPa to 35 MPa and a fixed temperature of 40 ˚C.

$$\rho=-3\times10^{-21}p^3+8\times10^{-14}p^2+7\times10^{-6}p-1.8655 \quad (3)$$

$$\mu=-3\times10^{-28}p^3+2\times10^{-20}p^2+6\times10^{-14}p+1\times10^{-5} \quad (4)$$

where p stands for pressure in Pa.

Slip flow is commonly presented in fluid flow in shale gas reservoirs. The slip velocity is defined as presented in Eq.5 [51, 52].

$$u_s = L_s \left(\frac{\partial u}{\partial n}\right)_s \quad (5)$$

where u_s is slip velocity in m/s, L_s presents the slip length in m, and n stands for the coordinate normal to the wall. In addition, the slip velocity is also presented in the form of Eq.6.

$$u_s - u_w = C_1 \lambda \left(\frac{\partial u}{\partial n}\right)_s \quad (6)$$

where u_s is slip velocity, u_w presents the surface/wall velocity. It is considered to be zero in this study because there is no wall movement. λ stands for the gas mean free path (methane molecules) which is a function of pressure, and C_1 stands for the slip coefficient, which is dependent on the tangential momentum accommodation coefficient (σ_v) and expressed as Eq.7. The value of 0.9 is used for σ_v in this study [53].

$$C_1 = \alpha_s \frac{2 - \sigma_v}{\sigma_v} \quad (7)$$

In Eq.7, α_s is a constant which is considered equal to one in the Maxwell model [54].

The desorption affects the properties of porous media, such as porosity, permeability, and pore radius. This effect can be described by the Langmuir theorem [55]. Eq.8 presents the detailed form of the Langmuir equation when it is converted into a volume unit.

$$vg = \frac{p \times vl}{p + pl} \times \rho_r \times h \times A \quad (8)$$

where vg presents gas content from the measured isotherm in m^3, vl stands for the Langmuir adsorbed gas in m^3/kg, ρ_r presents the rock density in kg/m^3, A presents the wall/rock/grain surface area in m^2 and h presents the wall/rock/grain thickness in m.

The adapted form of the Langmuir equation in cooperation with the mass balance equation is applied to the pores' wall as a boundary condition (Eq.9).

$$u_d = -\frac{vl \times \rho_r \times h}{\rho}\left[\rho \frac{d\left(\frac{p}{p+pl}\right)}{dp} + \frac{p}{p+pl}\frac{d\rho}{dp}\right]\frac{dp}{dt} \tag{9}$$

Needed for the above equation, Eq.3 is used to calculate the $\frac{d\rho}{dp}$ term. The rock density and rock thickness are assumed to be 2.4 g/cm and 4 microns, respectively [56]. Langmuir volume and pressure are extracted from the Heller and Zoback (2014) study for an Eagle Ford shale sample [57].

Governing equations are used to couple force equilibrium equations with the conservation of fluid mass. The equations include stress or strain factor that accounts for the poroelastic continuity equations, as well as the inclusion of pore pressure or fluid increment parameters that represents the fluid mass within the poroelastic system. To include the effect of stress in the presented model, the structural equations that are shown below are used to describe poroelasticity in the porous model based on the classical elasticity theory, which is derived in terms of shear moduli:

$$G\nabla^2 q + \frac{G}{1-2v}\left[\frac{\partial^2 q}{\partial x^2} + \frac{\partial^2 r}{\partial x \partial y}\right] + F_x - \alpha\frac{\partial p}{\partial x} = 0 \tag{10}$$

$$G\nabla^2 r + \frac{G}{1-2v}\left[\frac{\partial^2 q}{\partial y \partial x} + \frac{\partial^2 r}{\partial y^2}\right] + F_y - \alpha\frac{\partial p}{\partial y} = 0 \quad (11)$$

244 In Eqs 10-11, G is the shear modulus, q and r are displacements of solid (rock) in x and y
245 directions, and v is the Poisson ratio, α is Biot's constant, p is pore pressure.

246 The mechanical model solved in this study is then given through the following equations:

$$-\nabla \cdot \sigma = F_v\,, \sigma = S \quad (12)$$

$$S - s_0 = C : (\varepsilon - \varepsilon_0 - \varepsilon_{inel}) - \alpha p I \quad (13)$$

247 The strain is expressed in its index notation as shown in Eq.14.

$$\varepsilon_{ij} = \frac{1}{2}\left[\frac{\partial q_i}{\partial x_j} + \frac{\partial q_j}{\partial x_i}\right] \quad (14)$$

248 The stress tensors are denoted through σ and S, the volume force vector being expressed by
249 F_v, with the strain tensor term being ε and deformation vector term being q. The pore pressure
250 is denoted through the letter p, elastic tensor through the letter C and Biot's constant through
251 the term α. Subscript '0' describes initial values, whereas '$inel$' indicates the inelastic part of
252 the strain.

253 In the last step, Darcy's equation is used to calculate the apparent permeability of the whole
254 model, as presented in Eq.15.

$$K = \frac{V \times \Delta x \times \mu}{\Delta p} \tag{15}$$

where K presents apparent permeability of the porous media in D (Darcy), V presents the average velocity of gas in the pore network in cm/s, Δx stands for the length in the x-direction in cm, μ stands for viscosity in cp, and Δp is $(p_{inlet} - p_{outlet})$ in atm.

The above-mentioned equations were solved in an unsteady state condition using a finite element platform. To do so, the Stokes flow equation is solved by considering slip flow and gas adsorption as contributing terms in the boundary conditions. The inlet and outlet pressures of the pore network are assigned to be constant. Figure 4 shows the inlet (right side) and outlet (left side) boundaries as well as top and bottom boundaries (red lines). Pore walls are shown using blue lines where the slip flow and gas desorption are applied as boundary conditions using proper velocity term to the pore walls shown above. The pore pressure varies between 2500-3500 psi based on reported values of the pressure for the shale reservoir reservoirs [56]. The pressure gradient is set at 2 MPa/m (1.4 Pa/nm) [19]. The total simulation time is 2 seconds with a time step size of 0.1 seconds.

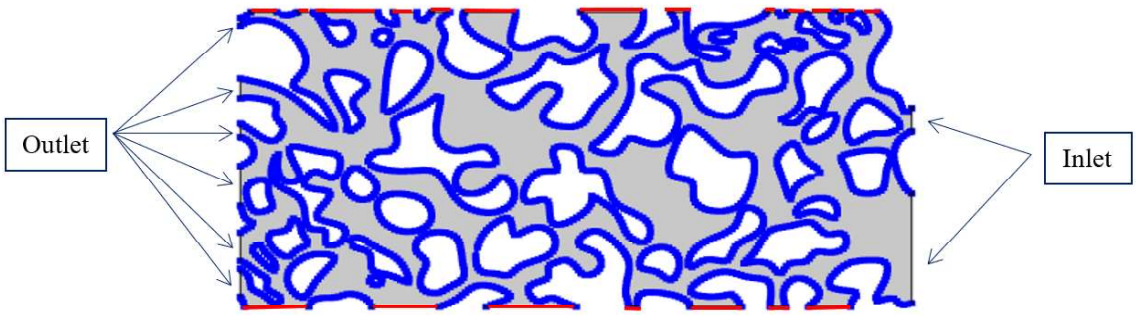

Figure 4. Pore network model

3. Results and discussion

This section discusses the flow dynamics considering slip flow and gas desorption under different effective stresses for a single pore model and a pore network model.

3.1 Single pore model

The single pore model was run under different effective stresses, where only the Stokes equation was used to describe the fluid flow (no slip or desorption). This case is set as a reference case to compare to cases that include the slip flow and gas desorption mechanisms later. The model was run with constant pore pressure of 13.8 MPa (2000 psi), while the effective stress was gradually increased from 3 MPa to 27 MPa (which is equivalent to 500 psi to 4000 psi) by increasing overburden pressure (loading stress). This range was chosen based on effective stress data gathered from Barnett and Eagle Ford shale reservoirs, where effective stress within Barnett shale reached levels up to 30 MPa [58]. Figure 5 shows the deformation of the pores' wall for the single pore model at the end of the simulation time. A deformation in pores' wall and contently in pore space could be noticed which was within the range of 4-10 nm. It is worth mentioning that, in this single pore system, the wall deformation has occurred almost in all directions, but more deformation can be observed horizontally (see Figure 5) causing the pore space change to be minimal.

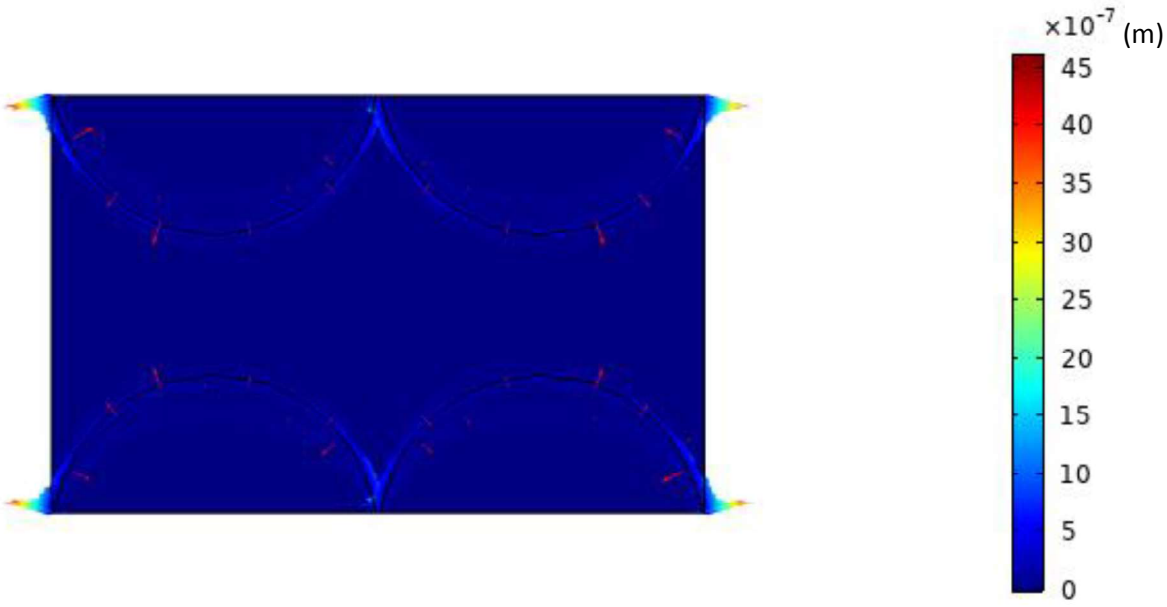

Figure 5. Deformation of the single pore model. The arrows point out the direction of the pore's wall deformation.

3.1.1 Effect of slip flow

The slip flow boundary condition is applied to the single pore model. Figure 6 compares permeability profiles at different effective stresses for two boundary conditions: 1) without the slip flow , and 2) with the slip flow .

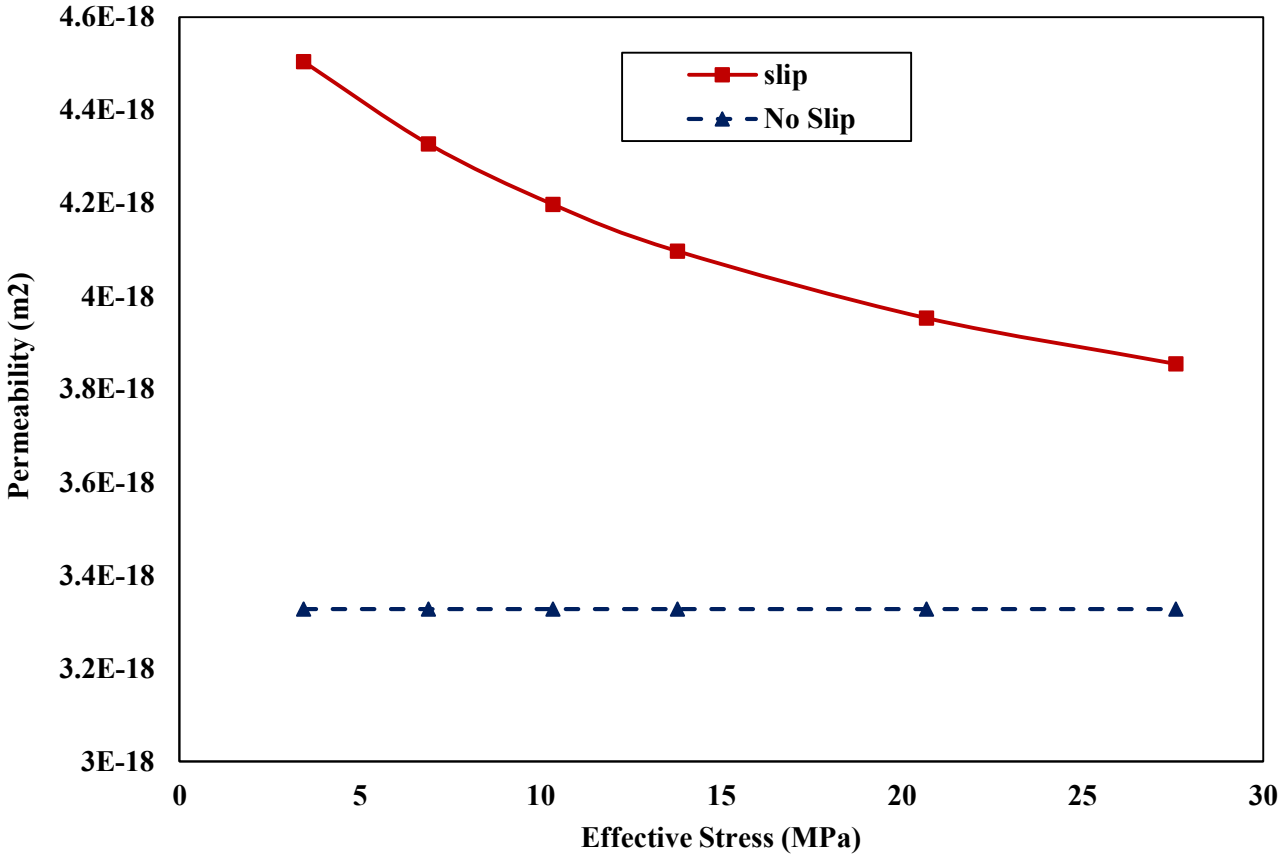

Figure 6. Single pore permeability profile for no-slip flow and slip flow conditions at different effective stresses

As shown in Figure 6, when effective stress increases the permeability values show insignificant changes for the no-slip flow condition. A 0.3% difference was observed by increasing effective stress from 3 MPa to 27 MPa. It is believed that this observation stems from the fact that the pore space change is minimal in this case as shown in Figure 5.

The permeability values are higher when the slip flow boundary is included. The slip flow leads to a 36% increase in permeability at the lowest-stress point compared to the no-slip case, while this value is 15% at the highest-stress condition. It should be noted that due to compression by increasing effective stress, the size of the pore reduces which is favorable for slip effect but at the same time, the pore pressure increases (due to pore space reduction) that

306 suppresses the slip effect. Considering the deformation is minimal here, pore pressure changes
307 would affect the slip flow physics more as compared to the pore size change. As a result, at
308 higher effective stress values, it is expected to have higher pore pressures (due to more
309 compression) and consequently have a lower slip flow contribution. This observation is in line
310 with the reported results in the literature, where it is mentioned that the effect of slip flow on
311 permeability is more dominated in lower pore pressure values [59, 60].

312 The permeability in the slip flow case is decreasing by 13% over increasing effective stress
313 to 27 MPa. The results show the slip flow mechanism is sensitive to stress because the slippage,
314 as a wall effect, can be influenced by wall deformation. It can also be noticed that with the
315 consideration of slip flow, the permeability trend shows an exponential behavior, where a
316 sharper trend of permeability reduction is observed at lower effective stresses due to higher
317 slip flow contribution.

318 ### 3.1.2 Coupled gas desorption and slip flow

319 The gas desorption is captured by the model through a velocity boundary condition term as
320 mentioned before. Figure 7 shows the permeability profiles induced by the gas desorption and
321 coupled slip flow and gas desorption for the Eagle Ford shale sample.

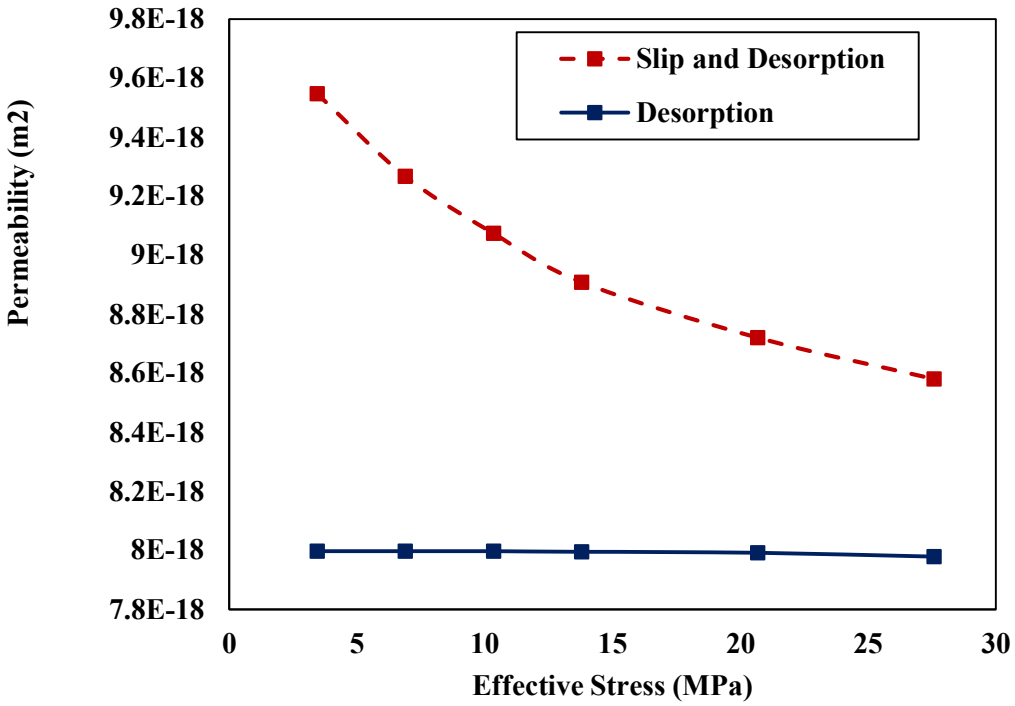

Figure 7. Permeability profile developed by gas desorption and slip flow mechanisms for different effective stresses (single pore model).

Figure 7 shows the permeability profiles developed by the consideration of the gas desorption mechanism alone, as well as the coupled effect of gas desorption and slip flow mechanisms against effective stress. In the case of gas desorption only, a negligible permeability reduction is observed by increase of effective stress and the reductions has mainly happened at higher effective stress values. As mentioned earlier, the desorption mechanism is controlled by the pressure difference between Langmuir pressure and pore pressure. Considering the fact that an increase in the effective stress leads to an increase in pore pressure, hence it is limiting the desorption mechanism. Even more, the reduction in pore space can be attributed to two factors, 1) reduction as a result of rock matrix deformation and 2) a reversal of the desorption effect due to high pressure. Therefore, the increase in pore pressure could lead to the adsorption of methane which would act as a further reduction in pore diameter, resulting in a steeper decline in permeability at higher effective stresses.

In the scenario in which both slip flow and gas desorption mechanisms are activated, the permeability profile follows a similar trend to that developed by the slip flow mechanism in Figure 6. This is expected as when the effect of stress on individual desorption and also on individual slip flow contribution was discussed above, it was observed that that stress has no

significant effect on desorption mechanism individually while it has shown a considerable effect on individual slip flow contribution. Nevertheless, a higher permeability reduction is observed when the slip and desorption effects are coupled as compared to individual slip effect case (comparing Figure 6 and Figure 7). This is because at higher effective stress values, desorption contribution will be reduced resulting in a sharper decrease in the apparat permeability curve of slip-desorption (Figure 7) as compared to curve of slip alone (Figure 6). Figures 8-10 show the velocity profile versus time for the three cases; slip flow acting alone, gas desorption acting alone and the coupled effect of slip flow and gas desorption to demonstrate the stress effect on these physics.

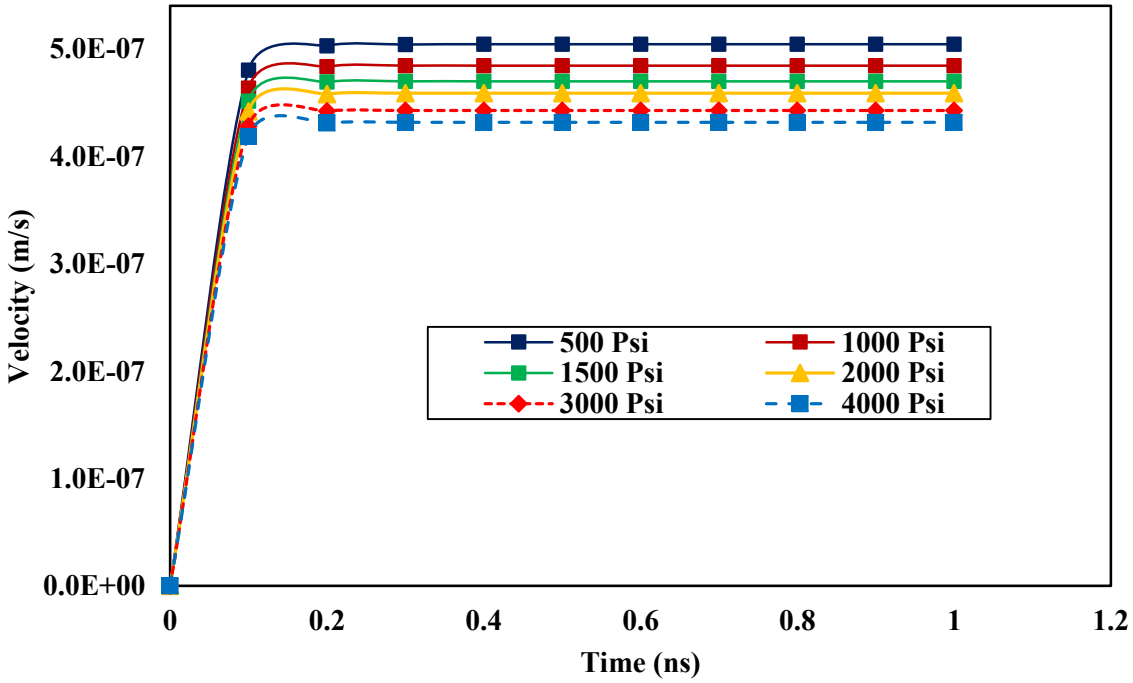

Figure 8. Velocity profile vs time under the effects of slip mechanism and stress effect

When considering the stress effect on the slip mechanism, as shown in Figure 8, it can be noted that as effective stress increases, the flow velocity decreases due to deformation at higher effective stresses. Results imply that higher stresses cause more compression of the gas due to pore size reduction, resulting in pore pressure increment while the velocity decreases to satisfy conservation of energy law. It also can be observed that, at the early stages of flow, the velocity

is increasing before becoming steady for all the applied effective stresses that shows a transient state due to gas compressibility at the beginning of the process.

Figure 9 shows the velocity profile for the scenario in which gas desorption is evaluated at different effective stresses showing insignificant effect of stress on desorption due to having almost the same velocity profile for all the stress cases. The general trend of velocity is increasing with time for all the effective stresses. A marginal reduction in velocity profiles can be observed in the simulation time between 0.1 ns and 0.3 ns. This highlights the fact that velocity has not reached a steady-state regime. Transnet behavior of flow is due to the transient nature of desorption mechanism.

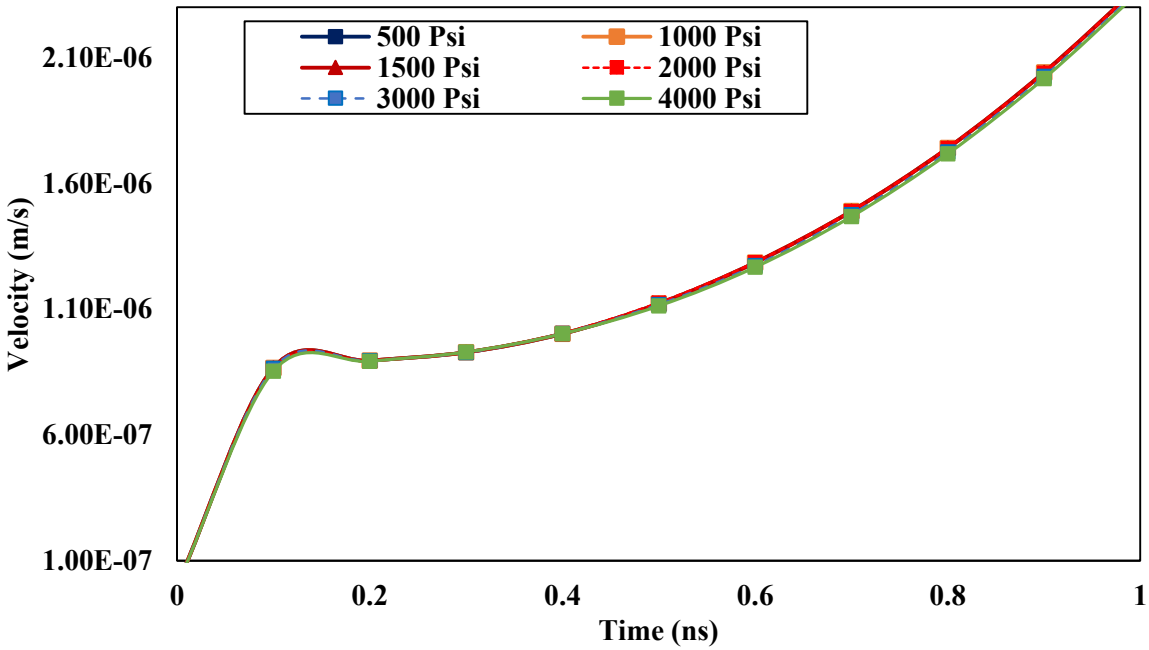

Figure 9. Velocity profile vs time under the effects of gas desorption mechanism and stress effect

Figure 10 shows the velocity profile when considering the combined effect of stress, slip flow, and gas desorption. Comparing with the Figure 9, the effect of stress is more recognizable in Figure 10 by looking at the curves that are not overlapping. As it can be observed, Figure 10 shows a higher velocity at lower stress values that is due to slip flow contribution (as also

observed in Figure 8). Additionally, Figure 10 illustrates that the velocity is increasing by time (a transient behavior) for all the applied stress values due to the contribution of the gas desorption (as also observed in Figure 9).

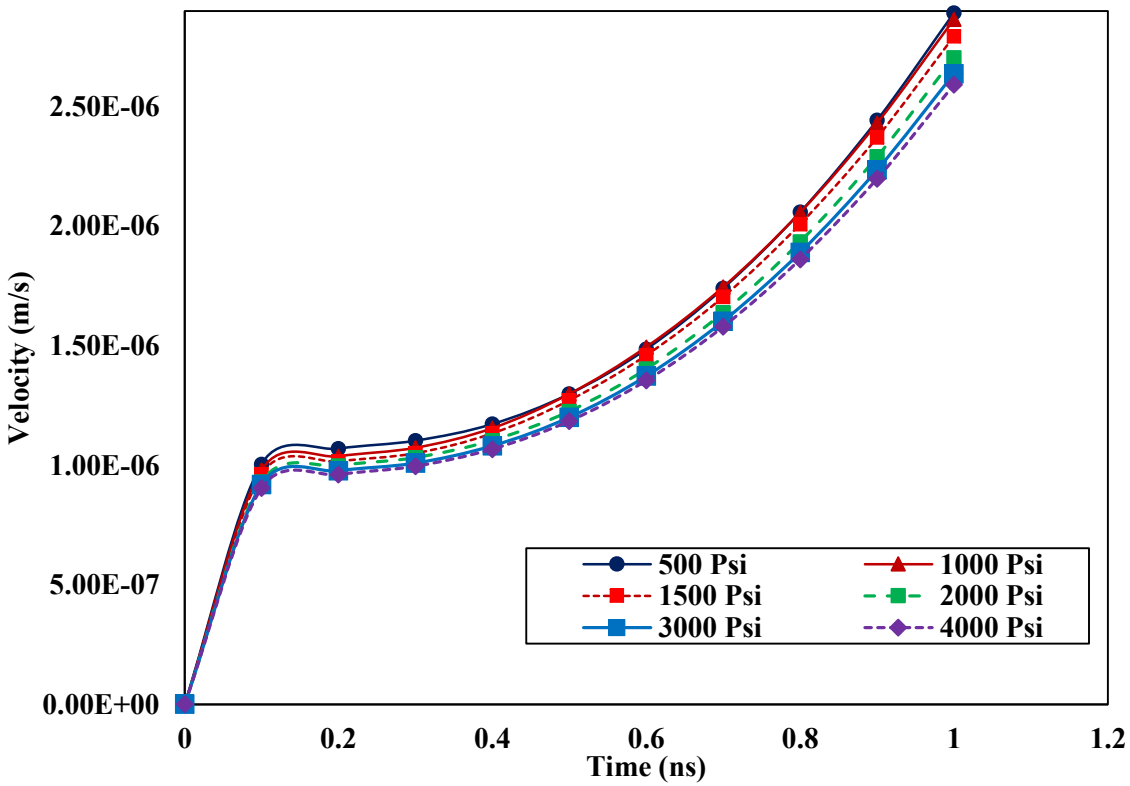

Figure 10. Velocity profile vs time under the coupled effects of slip flow, gas desorption, and stress effect

3.2 Pore network model

3.2.1 Slip flow

Similarly, using a pore network, the stress effect was investigated. Figure 11 shows the results of the base case (no slip flow or gas desorption) against the case slip flow case. It is expected that at high effective stresses, the resulting deformation causes an intensive gas compression, making the slip flow contribution to become minimal. As a result, the two curves in Figure 11 are expected to cross at high-stress values.

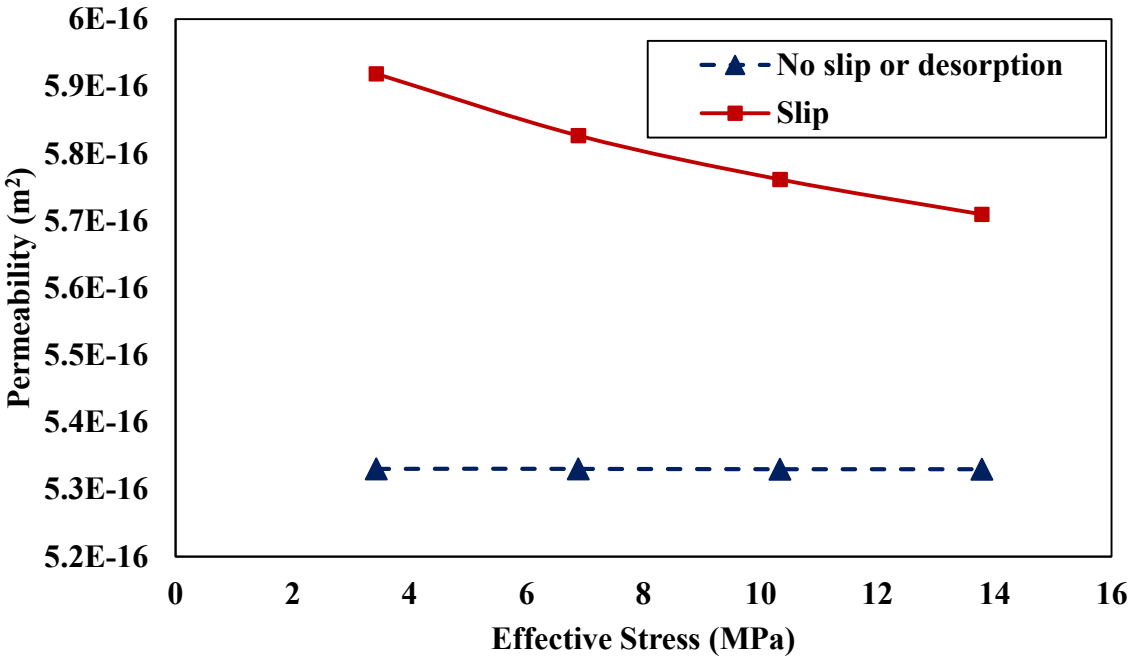

386
387 Figure 11. Pore network permeability profile for no-slip flow condition and slip flow at
388 different effective stresses

389 Figure 11 shows when fluid flow in the pore network is only affected by stress, the
390 permeability remains constant. It also shows a reducing trend in the permeability of the pore
391 network with respect to effective stress when the slip flow boundary is included. Increasing
392 effective stress causes a reduction in pores and pore throats radius, results in more contribution
393 of slip flow mechanism in fluid flow. A similar trend was observed when using the single pore
394 model (see Figure 6)

395 To verify the model performance, the results produced by the model while considering the
396 slip effect have been compared with experimental data gathered by Wei et al. (2018) on core
397 samples received from Longmaxi shale formation [61]. Figure 12 shows that the trend of
398 permeability profile predicted by the model is following the permeability trend obtained
399 experimentally for a different type of shale sample. The experiment was conducted under
400 constant injected gas pressure while loading pressure on the sample is gradually increased.

From the comparison, we can see that the expected behavioral trend obtained by our model follows the trend displayed by actual shale reservoirs. It should be noted that, as the shale sample used in the experiment is different from the sample checked by our model, it is not expected to get the same results. Nevertheless, predicting a similar trend with regard to stress effect is verifying that our model is set up properly.

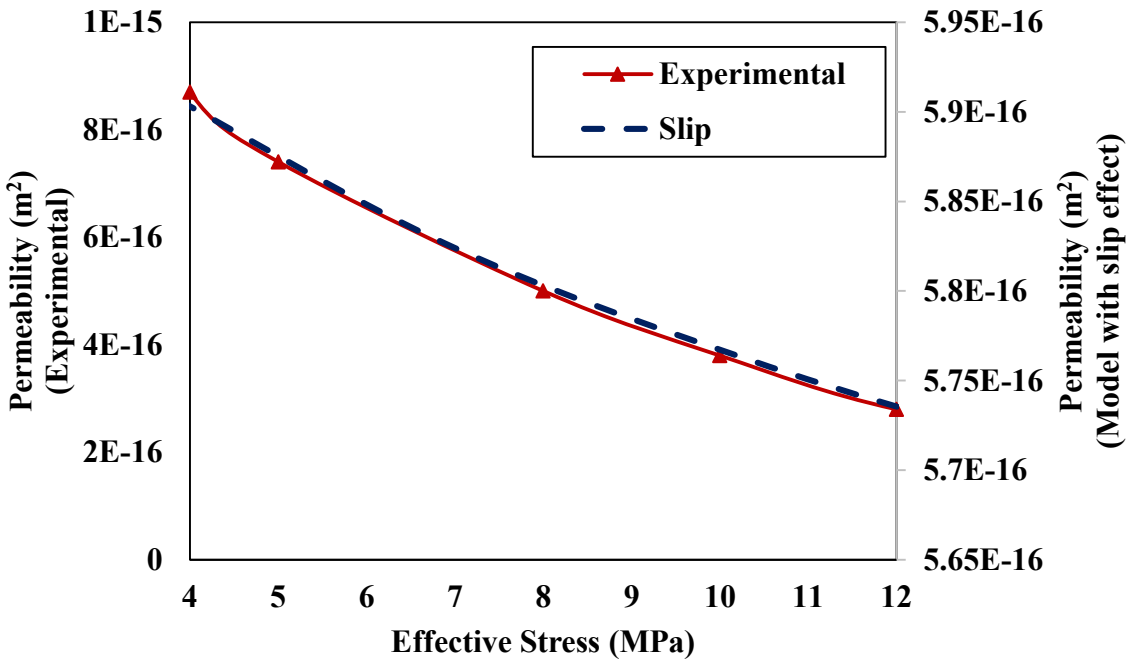

Figure 12. Permeability profile prediction by the model with slip effect compared to experimental data

3.2.2 Coupled gas desorption and slip flow effects

Figure 13 shows the permeability enhancement of a pore network due to slip flow, gas desorption, and coupled slip flow and gas desorption for an Eagle Ford shale sample.

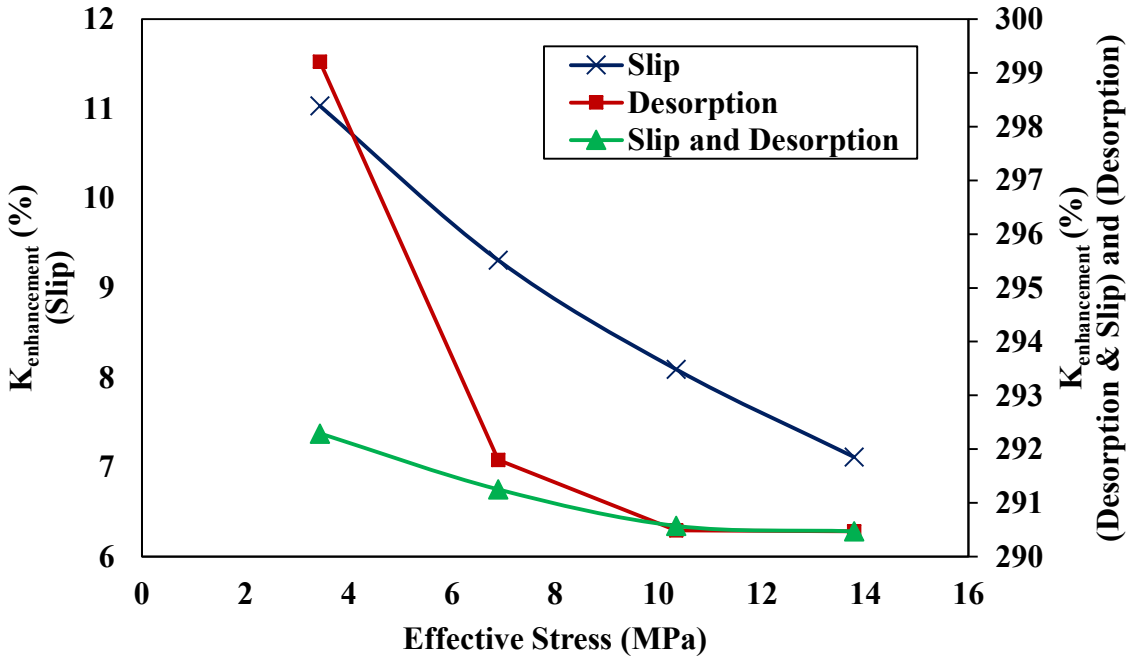

412
413 Figure 13. Permeability enhancement versus effective stress

414 Table 2 summarises the presented values of $K_{enhancement}$ (percent of permeability
415 enhancement relative to the permeability of the base case) in Figure 13 for different
416 mechanisms.

417 Table 2. Permeability alteration due to slip flow, gas desorption and coupled slip flow and
418 gas desorption under various stress effects for the Eagle Ford sample

Effective stress (MPa)	$K_{enhancement}$ by slip flow (%)	$K_{enhancement}$ by gas desorption (%)	$K_{enhancement}$ by slip flow and gas desorption (%)
3.45	11.03	299.21	292.29
6.89	9.31	290.50	291.25
10.34	8.09	290.49	290.57
13.79	7.11	290.47	290.47

419 At the lowest effective stress applied, i.e., 3.45 MPa (equivalent to 500 psi), the
420 enhancement due to the slip flow mechanism is 11%, and as effective stress was gradually
421 increased the enhancement is reduced to 7% at 13.79 MPa (equivalent to 2000 psi). There are
422 two reasons for reducing trend of permeability enhancement. First, the diameter of flow
423 channels is reducing with increasing effective stress. The second, the rise of pore pressure acts
424 to limit the slip flow effect.

425 The scenario in which gas desorption is encountered showed that it is more sensitive to stress
426 within the pore network. This stress-sensitive behavior was not captured by single pore model
427 due to exclusion of pore size and structure heterogeneity in the single pore model. At 3.45
428 MPa (equivalent to 500 psi) effective stress, the enhancement is 299%. However, it has dropped
429 to 290% as the effective stress increases to 6.89 MPa (equivalent to 1000 psi), and as effective
430 stress keeps increasing from 6.89 MPa to 13.79 MPa, the reduction of permeability is
431 insignificant (only 0.03%). This could be due to the Langmuir pressure limit. As the pressure
432 in the system rises beyond the Langmuir pressure, the desorption mechanism is reversed, and
433 methane gas starts to adsorb to the surface. The Langmuir pressure for Eagle ford shale is 4.8
434 MPa (approximately 700 psi). Therefore, the increase in effective stress acts to limit the gas
435 desorption effect as 6.89 MPa (equivalent to 1000 psi) stress was applied. The negligible
436 permeability reduction observed in the range of 6.89 MPa to 13.79 MPa is due to the formation
437 of an adsorbed layer that acts to further reduce or restrict the flow diameter. This observation
438 is consistent with Wang and Marongiu-Porcu (2015) study where they reported that the effect
439 of gas adsorption/desorption is significant when effective stress is small such as near the
440 fracture area in a fractured formation as having smaller effective stress magnitude compared
441 to spots in the matrix zone [62]. In addition, it is reported in the study by Taghavinejad et al.

(2020) that permeability remains almost constant at higher pressures when the adsorption layer is present [59].

The coupled effect of slip flow and gas desorption mechanisms show an enhancement of 292% at the applied 3.45 MPa (equivalent to 500 psi) stress and it falls to 290 % at 13.79 MPa (equivalent to 2000 psi) stress. The slip flow and gas desorption act oppositely when both of them are activated. It means that the magnitude of net permeability enhancement, which is due to slip flow and gas desorption, is not equal to the summation of the magnitude of the permeability enhancement due to individual slip flow and gas desorption. However, for higher stress values, as the slip flow mechanism becomes more limited, we can notice that the curve of coupled effect shows a closer matching to the curve of gas desorption alone. That is, slip flow effect is no longer limiting the gas desorption, hence we can see a closer matching between slip-desorption curve and desorption curve at higher stress values. In a study, Jia et al. (2020) investigated the stress-dependent permeability values under slip flow and coupled slip flow and gas desorption effects where a similar trend was observed verifying our results [60].

The inclusion of the stress term showed some notable results that help us understand the nature of the stress effect on shale gas flow. Our model (both single and pore network model) demonstrated that stress effect is limiting the gas flow in shale reservoirs by influencing both slip flow and gas desorption contributions. It should be noted that the contributions of slip flow and gas desorption are shown through an apparent permeability that represents the enhancement to the permeability of the base case (the model without slip flow and desorption terms). It was noted that the slip flow contribution would be limited by the stress effect. This is because, although the reduction in pore volume due to deformation acts in favor of the slip effect as gas-wall interaction increases, the resultant increase in pore pressure acts to limit the

slip effect as it restricts the mean free path of the flow. The sensitivity of the slip mechanism to additional stresses was noted when a small incrementation in effective stress showed a notable reduction in permeability enhancement. On the other hand, the effect of stress on the desorption term was noted at higher effective stress values. The reduction in permeability enhancement at low effective stresses was minor, this could be attributed to the gas adsorptive nature of shale that is a function of the pore pressure. The increase in effective stresses leads to an increase in pore pressure, which leads to the reversal of the desorption process into an adsorption process. This in return would reduce the permeability enhancement due to reduction of desorption contribution and furthermore would add to the reduction of pore space due to the formation of an adsorbed layer on the wall surface.

4. Conclusion

In this study, the gas flow behavior of the shale gas reservoirs is investigated in pore-scale in presence of slip flow, gas desorption, and the effect of stress. A typical single pore model and a pore network models using a down-scaled Berea sandstone image were created. Although the single pore model and pore network model produced almost similar trends of the mentioned mechanisms, they were slightly different. The differences are attributed to the pore-scale size and the additional heterogeneity found within the pore network model. Both models showed negative effect of stress on gas flow when slip flow and desorption mechanisms were activated in the models. In the single pore model, slip had a positive effect on desorption at a specific stress value when their coupled contributions were summative. However, the results of pore network model showed that slip had a destructive effect on desorption contribution specially at low effective stress values. It should be noted that, the flow in the model is controlled by a fixed differential pressure as constrained by the fixed inlet and outlet pressure boundary

conditions. As such, activating slip flow would result in having a higher pore pressure value compared to the base case regardless of the effective stress value. Therefore, the changes in pore pressure induced by the slip mechanism act to limit the desorption contribution. This was clearly noted with the consideration of stress effects. At high effective stress values, the slip effect is limited due to the increase in pore pressure by compression, hence we can notice a closer matching between the permeability enhancement produced by the desorption mechanism alone and the coupled effect of desorption and slip. Stress acts to limit the slip flow effect as well as the desorption mechanism as they both are a function of pore pressure, however, as stress increases the contribution of desorption is no longer reduced when both slip and desorption are activated.

References

[1] H. H. Liu, P. G. Ranjith, D. T. Georgi, and B. T. Lai, "Some key technical issues in modelling of gas transport process in shales: a review," *Geomechanics and Geophysics for Geo-Energy and Geo-Resources,* vol. 2, no. 4, pp. 231-243, 2016/12/01 2016.

[2] W. Shen, X. Li, Y. Xu, Y. Sun, and W. Huang, "Gas flow behavior of nanoscale pores in shale gas reservoirs," *Energies,* vol. 10, no. 6, p. 751, 2017.

[3] W. Song, J. Yao, J. Ma, G. Couples, and Y. Li, "Assessing relative contributions of transport mechanisms and real gas properties to gas flow in nanoscale organic pores in shales by pore network modelling," *International Journal of Heat and Mass Transfer,* vol. 113, pp. 524-537, 2017/10/01/ 2017.

[4] S. L. Thompson and W. R. Owens, "A survey of flow at low pressures," *Vacuum,* vol. 25, no. 4, pp. 151-156, 1975/04/01/ 1975.

[5] G. E. K. Ali Beskok, "Report: A Model for Flows in Channels, Pipes, and Ducts at Micro and Nano Scales," *Microscale Thermophysical Engineering,* vol. 3, no. 1, pp. 43-77, 1999/02/01 1999.

[6] L. J. Klinkenberg, "The Permeability Of Porous Media To Liquids And Gases," presented at the Drilling and Production Practice, New York, New York, 1941/1/1/, 1941. Available: https://doi.org/
[7] F. Civan, "Effective Correlation of Apparent Gas Permeability in Tight Porous Media," *Transport in Porous Media,* vol. 82, no. 2, pp. 375-384, 2010/03/01 2010.
[8] F. Javadpour, "Nanopores and Apparent Permeability of Gas Flow in Mudrocks (Shales and Siltstone)," *Journal of Canadian Petroleum Technology,* vol. 48, no. 08, pp. 16-21, 2009/8/1/ 2009.
[9] F. Javadpour, D. Fisher, and M. Unsworth, "Nanoscale Gas Flow in Shale Gas Sediments," *Journal of Canadian Petroleum Technology,* vol. 46, no. 10, p. 7, 2007/10/1/ 2007.
[10] E. Fathi and I. Y. Akkutlu, "Nonlinear Sorption Kinetics and Surface Diffusion Effects on Gas Transport in Low-permeability Formations," presented at the SPE Annual Technical Conference and Exhibition, New Orleans, Louisiana, 2009/1/1/, 2009. Available: https://doi.org/10.2118/124478-MS
[11] E. Fathi and I. Y. Akkutlu, "Lattice Boltzmann Method for Simulation of Shale Gas Transport in Kerogen," *SPE Journal,* vol. 18, no. 01, pp. 27-37, 2012/11/1/ 2012.
[12] S. M. Kang, E. Fathi, R. J. Ambrose, I. Y. Akkutlu, and R. F. Sigal, "Carbon Dioxide Storage Capacity of Organic-Rich Shales," *SPE Journal,* vol. 16, no. 04, pp. 842-855, 2011/12/1/ 2011.
[13] M. A. Ahmadi and S. R. Shadizadeh, "Experimental investigation of a natural surfactant adsorption on shale-sandstone reservoir rocks: Static and dynamic conditions," *Fuel,* vol. 159, pp. 15-26, 2015/11/01/ 2015.
[14] S. R. Etminan, F. Javadpour, B. B. Maini, and Z. Chen, "Measurement of gas storage processes in shale and of the molecular diffusion coefficient in kerogen," *International Journal of Coal Geology,* vol. 123, pp. 10-19, 2014/03/01/ 2014.
[15] F. Yang, Z. Ning, R. Zhang, H. Zhao, and B. M. Krooss, "Investigations on the methane sorption capacity of marine shales from Sichuan Basin, China," *International Journal of Coal Geology,* vol. 146, pp. 104-117, 2015/07/01/ 2015.
[16] W. X. She, J. B. Chen, J. Zhang, B. Wei, H. Q. Wang, and R. Bai, "The Calculation of Apparent Permeability for Shale Gas Considering Adsorption and Flow Patterns," *Advanced Materials Research,* vol. 1073-1076, pp. 2305-2309, 2015.
[17] J. Wang, H. Luo, H. Liu, J. Lin, L. Li, and W. Lin, "Influences of adsorption/desorption of shale gas on the apparent properties of matrix pores," *Petroleum Exploration and Development,* vol. 43, no. 1, pp. 158-165, 2016/02/01/ 2016.
[18] Y. Zhang, D. Li, X. Sun, Z. Song, D. Shi, and Y. Su, "A new model for calculating the apparent permeability of shale gas in the real state," *Natural Gas Industry B,* vol. 5, no. 3, pp. 245-252, 2018/06/01/ 2018.
[19] J. Foroozesh, A. I. M. Abdalla, and Z. Zhang, "Pore Network Modeling of Shale Gas Reservoirs: Gas Desorption and Slip Flow Effects," *Transport in Porous Media,* vol. 126, no. 3, pp. 633-653, 2019/02/01 2019.
[20] K. Terazaghi, "Theoretical soil mechanics," *John Wiley and Sons,* 1965.
[21] M. A. Biot, "Mechanics of Deformation and Acoustic Propagation in Porous Media," *Journal of Applied Physics,* vol. 33, no. 4, pp. 1482-1498, 1962/04/01 1962.
[22] C. An, J. Killough, and L. Mi, "Stress-dependent permeability of organic-rich shale reservoirs: Impacts of stress changes and matrix shrinkage," *Journal of Petroleum Science and Engineering,* vol. 172, pp. 1034-1047, 2019/01/01/ 2019.

[23] J.-J. Dong *et al.*, "Stress-dependence of the permeability and porosity of sandstone and shale from TCDP Hole-A," *International Journal of Rock Mechanics and Mining Sciences,* vol. 47, no. 7, pp. 1141-1157, 2010/10/01/ 2010.
[24] D. Zivar, J. Foroozesh, P. Pourafshary, and S. Salmanpour, "Stress dependency of permeability, porosity and flow channels in anhydrite and carbonate rocks," *Journal of Natural Gas Science and Engineering,* vol. 70, p. 102949, 2019/10/01/ 2019.
[25] D. Zivar, S. Shad, J. Foroozesh, and S. Salmanpour, "Experimental study of sand production and permeability enhancement of unconsolidated rocks under different stress conditions," *Journal of Petroleum Science and Engineering,* vol. 181, p. 106238, 2019/10/01/ 2019.
[26] R. L. Kranzz, A. D. Frankel, T. Engelder, and C. H. Scholz, "The permeability of whole and jointed Barre Granite," *International Journal of Rock Mechanics and Mining Sciences & Geomechanics Abstracts,* vol. 16, no. 4, pp. 225-234, 1979/08/01/ 1979.
[27] A. F. Gangi, "Variation of whole and fractured porous rock permeability with confining pressure," *International Journal of Rock Mechanics and Mining Sciences & Geomechanics Abstracts,* vol. 15, no. 5, pp. 249-257, 1978/10/01/ 1978.
[28] Z. Pan, Y. Ma, L. D. Connell, D. I. Down, and M. Camilleri, "Measuring anisotropic permeability using a cubic shale sample in a triaxial cell," *Journal of Natural Gas Science and Engineering,* vol. 26, pp. 336-344, 2015/09/01/ 2015.
[29] S. Li, D. Tang, Z. Pan, H. Xu, and W. Huang, "Characterization of the stress sensitivity of pores for different rank coals by nuclear magnetic resonance," *Fuel,* vol. 111, pp. 746-754, 2013/09/01/ 2013.
[30] Y. Tan, Z. Pan, X.-T. Feng, D. Zhang, L. D. Connell, and S. Li, "Laboratory characterisation of fracture compressibility for coal and shale gas reservoir rocks: A review," *International Journal of Coal Geology,* vol. 204, pp. 1-17, 2019/03/01/ 2019.
[31] D. Yang, W. Wang, W. Chen, S. Wang, and X. Wang, "Experimental investigation on the coupled effect of effective stress and gas slippage on the permeability of shale," *Scientific Reports,* vol. 7, no. 1, p. 44696, 2017/03/17 2017.
[32] D. J. Soeder, "Porosity and Permeability of Eastern Devonian Gas Shale," *SPE Formation Evaluation,* vol. 3, no. 01, pp. 116-124, 1988/3/1/ 1988.
[33] M. Gutierrez, D. Katsuki, and A. Tutuncu, "Determination of the continuous stress-dependent permeability, compressibility and poroelasticity of shale," *Marine and Petroleum Geology,* vol. 68, pp. 614-628, 2015/12/01/ 2015.
[34] R. M. Bustin, A. M. M. Bustin, A. Cui, D. Ross, and V. M. Pathi, "Impact of Shale Properties on Pore Structure and Storage Characteristics," presented at the SPE Shale Gas Production Conference, Fort Worth, Texas, USA, 2008/1/1/, 2008. Available: https://doi.org/10.2118/119892-MS
[35] Z. Wentong, W. Qing, N. Zhengfu, Z. Rui, H. Liang, and C. Zhilin, "Relationship between the stress sensitivity and pore structure of shale," *Journal of Natural Gas Science and Engineering,* vol. 59, pp. 440-451, 2018/11/01/ 2018.
[36] R. Nazari Moghaddam and M. Jamiolahmady, "Fluid transport in shale gas reservoirs: Simultaneous effects of stress and slippage on matrix permeability," *International Journal of Coal Geology,* vol. 163, pp. 87-99, 2016/06/01/ 2016.
[37] Z. Sun, X. Li, J. Shi, T. Zhang, and F. Sun, "Apparent permeability model for real gas transport through shale gas reservoirs considering water distribution characteristic," *International Journal of Heat and Mass Transfer,* vol. 115, pp. 1008-1019, 2017/12/01/ 2017.

[38] X. Feng, F. Ma, H. Zhao, G. Liu, and J. J. S. Guo, "Gas multiple flow mechanisms and apparent permeability evaluation in shale reservoirs," vol. 11, no. 7, p. 2114, 2019.
[39] A. Shabani, D. Zivar, H. R. Jahangiri, and A. Shahrabadi, "Application of pore network modeling in deep bed filtration analysis," *SN Applied Sciences,* vol. 2, no. 9, p. 1537, 2020/08/19 2020.
[40] H. Yu, Y. Zhu, X. Jin, H. Liu, and H. Wu, "Multiscale simulations of shale gas transport in micro/nano-porous shale matrix considering pore structure influence," *Journal of Natural Gas Science and Engineering,* vol. 64, pp. 28-40, 2019/04/01/ 2019.
[41] I. Fatt, "The Network Model of Porous Media," *Transactions of the AIME,* vol. 207, no. 01, pp. 144-181, 1956/12/1/ 1956.
[42] H. Darabi, A. Ettehad, F. Javadpour, and K. Sepehrnoori, "Gas flow in ultra-tight shale strata," *Journal of Fluid Mechanics,* vol. 710, pp. 641-658, 2012.
[43] H.-H. Liu, D. Georgi, and J. Chen, "Correction of source-rock permeability measurements owing to slip flow and Knudsen diffusion: a method and its evaluation," *Petroleum Science,* vol. 15, no. 1, pp. 116-125, 2018/02/01 2018.
[44] W. Song, J. Yao, J. Ma, Y. Li, and W. Han, "A pore structure based real gas transport model to determine gas permeability in nanoporous shale," *International Journal of Heat and Mass Transfer,* vol. 126, pp. 151-160, 2018/11/01/ 2018.
[45] C. L. Cipolla, E. P. Lolon, J. C. Erdle, and V. Tathed, "Modeling Well Performance in Shale-Gas Reservoirs," presented at the SPE/EAGE Reservoir Characterization & Simulation Conference, Oct 2009, 2009. Available: https://www.earthdoc.org/content/papers/10.3997/2214-4609-pdb.170.spe125532
[46] A. Sakhaee-Pour and S. Bryant, "Gas Permeability of Shale," *SPE Reservoir Evaluation & Engineering,* vol. 15, no. 04, pp. 401-409, 2012/8/1/ 2012.
[47] A. A. Keller, M. J. Blunt, and A. P. V. Roberts, "Micromodel observation of the role of oil layers in three-phase flow," *Transport in Porous Media,* vol. 26, no. 3, pp. 277-297, 1997.
[48] G. K. Batchelor, *An introduction to fluid dynamics*. Cambridge university press, 2000.
[49] S. Kim and S. J. Karrila, *Microhydrodynamics: principles and selected applications*. Courier Corporation, 2013.
[50] E. W. Lemmon, M. O. McLinden, and D. G. Friend, "Thermophysical Properties of Fluid Systems," in *NIST Chemistry WebBook, NIST Standard Reference Database Number 69*: National Institute of Standards and Technology, Gaithersburg MD, 20899.
[51] R. N. Moghaddam, S. Aghabozorgi, and J. Foroozesh, "Numerical Simulation of Gas Production From Tight, Ultratight and Shale Gas Reservoirs: Flow Regimes and Geomechanical Effects," presented at the EUROPEC 2015, Madrid, Spain, 2015/6/1/, 2015. Available: https://doi.org/10.2118/174323-MS
[52] R. Nazari Moghaddam and M. Jamiolahmady, "Slip flow in porous media," *Fuel,* vol. 173, pp. 298-310, 2016/06/01/ 2016.
[53] G. Karniadakis, A. Beskok, and N. Aluru, *Microflows and nanoflows: fundamentals and simulation*. Springer Science & Business Media, 2006.
[54] W.-M. Zhang, G. Meng, and X. Wei, "A review on slip models for gas microflows," *Microfluidics and Nanofluidics,* vol. 13, no. 6, pp. 845-882, 2012/12/01 2012.
[55] I. Langmuir, "The Constitution and Fundamental Properties of Solids and Liquids. Part I. Solids," *Journal of the American Chemical Society,* vol. 38, no. 11, pp. 2221-2295, 1916/11/01 1916.
[56] E. Crain, *Crain's petrophysical handbook*. Spectrum 2000 Mindware Limited, 2002.

[57] R. Heller and M. Zoback, "Adsorption of methane and carbon dioxide on gas shale and pure mineral samples," *Journal of Unconventional Oil and Gas Resources,* vol. 8, pp. 14-24, 2014/12/01/ 2014.
[58] H. Sone and M. D. Zoback, "Mechanical properties of shale-gas reservoir rocks — Part 1: Static and dynamic elastic properties and anisotropy," *GEOPHYSICS,* vol. 78, no. 5, pp. D381-D392, 2013/09/01 2013.
[59] A. Taghavinejad, M. Sharifi, E. Heidaryan, K. Liu, and M. Ostadhassan, "Flow modeling in shale gas reservoirs: A comprehensive review," *Journal of Natural Gas Science and Engineering,* vol. 83, p. 103535, 2020/11/01/ 2020.
[60] B. Jia, J.-S. Tsau, and R. Barati, "Investigation of Shale-Gas-Production Behavior: Evaluation of the Effects of Multiple Physics on the Matrix," *SPE Reservoir Evaluation & Engineering,* vol. 23, no. 01, pp. 068-080, 2020.
[61] C. Wei *et al.*, "A study of nonlinear elasticity effects on permeability of stress sensitive shale rocks using an improved coupled flow and geomechanics model: a case study of the Longmaxi shale in China," *Energies,* vol. 11, no. 2, p. 329, 2018.
[62] H. Wang and M. Marongiu-Porcu, "Impact of Shale-Gas Apparent Permeability on Production: Combined Effects of Non-Darcy Flow/Gas Slippage, Desorption, and Geomechanics," *SPE Reservoir Evaluation & Engineering,* vol. 18, no. 04, pp. 495-507, 2015.